Earth Syst. Dynam. Discuss., 4, 967–1003, 2013
www.earth-syst-dynam-discuss.net/4/967/2013/
doi:10.5194/esdd-4-967-2013

Earth System Dynamics Discussions
Open Access

The role of the North Atlantic overturning and deep-ocean for multi-decadal global-mean-temperature variability

C. F. Schleussner[1,2], **J. Runge**[1,3], **J. Lehmann**[1,2], **and A. Levermann**[1,2]

[1]Potsdam Institute for Climate Impact Research, Telegrafenberg A62, 14473 Potsdam, Germany
[2]Physics Institute, Potsdam University, Potsdam, Germany
[3]Department of Physics, Humboldt University, Berlin, Germany

Received: 7 August 2013 – Accepted: 11 August 2013 – Published: 6 September 2013

Correspondence to: C. F. Schleussner (schleussner@pik-potsdam.de)

Published by Copernicus Publications on behalf of the European Geosciences Union.

Abstract

Earth's climate exhibits internal modes of variability on various time scales. Here we investigate multi-decadal variability of the Atlantic meridional overturning circulation (AMOC) in the control runs of an ensemble of CMIP5 models. By decomposing global-mean-temperature (GMT) variance into contributions of the AMOC and Northern Hemisphere sea-ice extent using a graph-theoretical statistical approach, we find the AMOC to contribute 8 % to GMT variability in the ensemble mean. Our results highlight the importance of AMOC sea-ice feedbacks that explain 5 % of the GMT variance, while the contribution solely related to the AMOC is found to be about 3 %. As a consequence of multi-decadal AMOC variability, we report substantial variations in North Atlantic deep-ocean heat content with trends of up to 0.7×10^{22} J decade^{-1} that are of the order of observed changes over the last decade and consistent with the reduced GMT warming trend over this period. Although these temperature anomalies are largely density-compensated by salinity changes, we find a robust negative correlation between the AMOC and North Atlantic deep-ocean density with density lagging the AMOC by 5 to 11 yr in most models. While this would in principle allow for a self-sustained oscillatory behavior of the coupled AMOC–deep-ocean system, our results are inconclusive about the role of this feedback in the model ensemble.

1 Introduction

Multi-decadal variability of the climate system has been studied intensively, with a special focus on the last millennium and climate variability on centennial time scales (e.g., Eby et al., 2012; Fernández-Donado et al., 2013; Ortega et al., 2011; Fidel et al., 2011; Otterå et al., 2010; Hofer et al., 2011). Among others, a dominant mode of global climate variability is the Atlantic multi-decadal oscillation (AMO) (Schlesinger and Ramankutty, 1994) in the North Atlantic that is evident in ocean records over the last 8000 yr (Knudsen et al., 2011). The AMO as a signal of anomalous sea-surface tem-

ESDD
4, 967–1003, 2013

peratures in the North Atlantic has been found to have profound influence on other climate phenomena, e.g. Atlantic hurricane frequency (Vimont and Kossin, 2007; Zhang and Delworth, 2009), West African Monsoon and Sahel rainfall (Mohino et al., 2010).

Model studies suggest that the multi-decadal mode in North Atlantic sea-surface temperatures (SSTs) is closely related to variability of the Atlantic meridional overturning circulation (AMOC) (Timmermann and Latif, 1998; Knight et al., 2005; Delworth et al., 2007; Park and Latif, 2011; Ba et al., 2013) with models exhibiting AMOC variability on multi-decadal to multi-centennial time scales (Menary et al., 2011; Wouters et al., 2012). The origin of these multi-decadal modes is not jet fully understood. Already simple box-models are found to produce multi-decadal variability as a result of delayed advection (Griffies and Tziperman, 1995; Lee and Wang, 2010) and Dijkstra et al. (2006) report a multi-decadal mode in models of different complexity driven by horizontal temperature anomalies (Te Raa and Dijkstra, 2002; Sévellec and Fedorov, 2013). By analyzing observational records, Dima and Lohmann (2010) find two distinct modes in observed Atlantic SST over the last century. Consistently, Park and Latif (2008) report multiple modes of AMOC variability in the Kiel Climate Model with a multi-centennial mode originating in the Southern Ocean and a multi-decadal one of Northern Hemisphere origin.

While several model studies find stochastic atmospheric forcing to be the dominant driver (Eden and Willebrand, 2001; Tulloch and Marshall, 2012) of the Northern Hemisphere variability component, others report variations in Labrador Sea convection as a possible origin (Bentsen et al., 2004; Medhaug et al., 2011; Persechino et al., 2012). Delworth and Zeng (2012) and Ba et al. (2013) find salinity advection to drive variability in Labrador sea convection, where salinity anomalies of subtropical and arctic origin are found to play a role (Jungclaus et al., 2005). Born et al. (2012) identified this salinity advection feedback on subpolar convection as a potential driver of multi-stability of the horizontal subpolar gyre circulation (Levermann and Born, 2007) in a multi-model study. The existence of such a multi-stability was found to greatly enhance subpolar variability close to the system's internal threshold (Mengel et al., 2012).

ESDD
4, 967–1003, 2013

Atlantic variability is found to significantly contribute to Northern Hemisphere variations (Zhang et al., 2007; Knight et al., 2005, 2006) and eventually to global mean temperature (GMT). Zanchettin et al. (2010) find multi-decadal AMOC variations to be a major source of GMT variability over the last millennium and Feulner et al. (2013) report meridional heat transport in the Atlantic to be the dominant process behind the persistent temperature difference between Northern and Southern Hemisphere in an unperturbed climate. In a multi-model intercomparison, Jones et al. (2013) suggest multi-decadal variability in the high northern latitudes to be a major source of deviations within the CMIP5 model ensemble and in comparison with observational data over the 20th century. Besides oceanic contribution, sea- ice retreat has been a dominant contributor to observed northern high-latitude warming over the recent decades (Holland and Bitz, 2003; Screen and Simmonds, 2010).

Here, we first disentangle the contributions of AMOC and sea-ice variability to GMT variations in unperturbed control runs of the CMIP5 model ensemble using graph-theoretical statistical models (Runge et al., 2012a; Ebert-Uphoff and Deng, 2012, denoted graphical models hereafter) and commonality analysis (Seibold and McPhee, 1979). Then we relate AMOC variability to North Atlantic deep-ocean temperature and salinity and investigate an internal advective feedback mechanism. The magnitude of the deep-ocean warming rate that is found in the CMIP5 models is consistent with the observed changes over the past decade. The link between GMT reduction and deep-ocean warming is quantitatively consistent with the past reduction in the GMT warming trend.

2 Temperature-circulation relations in the climate model ensemble CMIP-5

We analyze the unperturbed control run of seven Atmosphere Ocean General Circulation Models (AOGCMs) from the coupled model intercomparison project CMIP5 (Taylor et al., 2012) that provide all diagnostics required for our analysis and at minimum 300 yr of model data. Figure 1 shows the time series for GMT, AMOC, AMO

ESDD
4, 967–1003, 2013

and Northern Hemisphere sea-ice extent (SIE) as well as North Atlantic Deep Ocean (NADO) temperature (45° to 65° N, z = 1000–2000 m). The AMOC is derived as the vertical maximum of the streamfunction at 45° N and the AMO as the anomaly of Atlantic SSTs between 30° and 65° N. The corresponding power spectra are depicted in Fig. 2. We find two coherent modes in AMOC, GMT and SIE for the MPI-ESM-LR (-MR) model with around 30 and 40 (45) yr period, that are significant at the 95 % level. The CanESM2 spectrum also exhibits significant AMOC modes at around 25 and 40 yr, whereas only the 25 yr mode is present also in the GMT and SIE spectra, though not significant at the 95 % level. A 25 yr mode is also present in the CNRM-CM5 spectrum.

The time series of all other models are considerably shorter (500 yr or less), which reduces the signal to noise ratio and thus leads to less or no significant spectral peaks. Despite that, the AMOC spectrum for the CESM1-BGC exhibits significant AMOC modes at around 30 and 60 yr.

Cross-correlations between the AMOC and AMO, GMT and SIE reveal a clear relation between AMO and AMOC in all models with some models exhibiting an AMOC lead by several years (Fig. 3). We also find a robust positive correlation at zero or one year lag between AMOC and GMT significant at the 95 % significance level as well as a negative peak between AMOC and SIE. The cross-correlation for the AMOC and GMT in CNRM-CM5 model are significant, but do not exhibit a clear peak as a consequence of a very weak AMOC mean state and weak variability on less than centennial time scales in this model (compare Fig. 1).

Significant cross-correlation does, however, not imply physical relevance. To test for the importance of the high northern latitudes for absolute GMT variability, we derived the latitude dependent contribution of surface air temperature (SAT) anomalies to the GMT signal. Figure 4 depicts the explained variance (R^2) of the GMT time series by the zonal and meridional integrated SAT anomalies north of the latitude drawn on the x axis. The expected surface area contribution by latitude assuming SAT anomalies to be uniform across the globe, is drawn for comparison (in grey). We find about one third of the GMT variance to originate north of 45° N in the ensemble mean exceeding their

ESDD
4, 967–1003, 2013

share expected purely by the surface area. We applied a forward-backward butterworth low-pass filter with cut-off frequencies from 10 to 50 yr to our time series and find the northern latitude contribution to increase with increased filtering in all models except the CCSM4 and CNRM-CM5. Half of the multi-decadal GMT variance in the MPI-ESM-LR originates north of 45° N and we hypothesize AMOC and SIE as likely drivers. The CCSM4 actually shows a decrease for multi-decadal variability, but our analysis suggests the high latitudes of the Southern Hemisphere to be dominant contributors to GMT variability in this model (compare Fig. 4). Thus, our results indicate that the high northern latitudes are indeed an important contributor to GMT variability on annual time scales and that this share increases for multi-decadal variability. We performed the same analysis with an ensemble of 30 CMIP5 models (not shown) confirming our results.

3 Quantifying AMOC contributions to GMT variance

Cross correlations need to be interpreted cautiously, since they are subject to several limitations. In the presence of strong auto-correlation, peaks in the cross-correlation can be amplified and shifted to larger time lags, limiting the interpretability of time delays in such systems (Runge et al., 2013). Additionally, in the global climate system with its complex coupled dynamic, also common driver effects and indirect chains can occur. A notional process Z that drives two processes X and Y is called a common driver of X and Y, whereas an indirect chain is present if process X drives Z and Z drives Y, without a direct relation between X and Y. In both cases, a non-zero cross-correlation between X and Y would be detected, even though no direct interaction is present.

ESDD
4, 967–1003, 2013

3.1 Graphical model analysis

To overcome these limitations, graphical models can be used to identify causal relations in complex coupled systems (Ebert-Uphoff and Deng, 2012). Here we apply a graphical model approach introduced by Runge et al. (2012a,b). While this approach is also applicable to nonlinear interactions, here the linear case as discussed in Runge et al. (2013) is used to determine linear causal interdependencies. In the following, we illustrate the concept with a simple example and refer to the references for further details on the methodology.

Consider the simple bivariate first order auto-regressive stochastic process (AR(1))

$$X_t = a\, X_{t-1} + \epsilon_t^X \qquad (1)$$
$$Y_t = cX_{t-1} + bY_{t-1} + \epsilon_t^Y.$$

where X and Y denote the two variables of the stochastic process and a, b and c are constant coefficients. The coefficients a and b represent the auto-regressive contribution of X and Y respectively and $|a|, |b| < 1$ is required for the process to be stationary. c gives the coupling between the two and can in principle attain any finite value. $(\epsilon_t^X, \epsilon_t^Y)$ are independent identically distributed Gaussian random variables with a given covariance matrix

$$\mathbf{\Sigma} = \begin{pmatrix} \sigma_X^2 & \sigma_{XY} \\ \sigma_{XY} & \sigma_Y^2 \end{pmatrix} \qquad (2)$$

and zero mean.

A time series graph for this model can be constructed, where the nodes are represented by the time-dependent states X_t, Y_t, X_{t-1}, Y_{t-1}, (...). *Directed* links (symbolized by $\rightarrow$) are given by non-zero coefficients a, b, c and undirected *contemporaneous* links are given by non-zero entries in the inverse covariance matrix $\mathbf{\Sigma}$. This time series graph for our model system is illustrated in Fig. 5. Note that time series stationarity as a pre-

ESDD
4, 967–1003, 2013

requisite for such an analysis implies that if "$X_{t-\tau} \to Y_t$", "$X_{t'-\tau} \to Y_{t'}$" is true for any t'.

In real world systems, however, the exact relations between the investigated processes are often unknown and a time series graph algorithm as introduced in Runge et al. (2012b) can help to identify causalities in such complex coupled systems. As an illustration, consider the estimation of the parents of Y in the time series graph shown in Fig. 5. The algorithm tests possible links from all processes (including Y) at all lags up to a maximum delay (that can be speci ed accordingly, for the analysis presented below we use a maximum time lag of 30 yr). Here the hypothetical link "$X_{t-2} \to Y_t$" would be tested by first checking whether the unconditional cross correlation $\rho(X_{t-2}; Y_t)$ is nonzero. Since there exists a path between X_{t-2} and Y_t, this will be the case. In the next iteration step, the conditional linear dependence is tested. As a heuristic for selecting the conditions in each test, we choose the conditions sorted by their correlation value in the previous step. Assuming $\rho(Y_{t-1}; Y_t) > \rho(X_{t-1}; Y_t) > \ldots$ in our example, the partial correlation $\rho(X_{t-2}; Y_t | Y_{t-1})$ that excludes the influence of Y_{t-1}, would be tested. This partial correlation would also be non-zero due to the unblocked path "$X_{t-2} \to X_{t-1} \to Y_t$". Also the test with the next-largest condition on X_{t-1} yields a non-zero partial correlation. After some more tests with weaker conditions, the partial correlation $\rho(X_{t-2}; Y_t | Y_{t-1}, X_{t-1})$ would be found to vanish, such that the hypothetical link can be removed. An analogue procedure is applied for contemporaneous links, where all directed links identified and iteratively more and more contemporaneous links are conditioned out (Runge et al., 2012b).

Following this procedure, we now construct a time series graph for GMT, AMOC and SIE with a two-sided significance level of 99 % for the partial correlation test. The resulting cross-links between AMOC, GMT and SIE are illustrated in Fig. 6. Across the whole ensemble, we robustly find contemporaneous links with a positive partial correlation between AMOC and GMT and a negative partial correlation between SIE and GMT. Several models also show negative "GMT → SIE" and "SIE → GMT" links at a time lag of one year. On the one hand sea-ice reduction will lead to atmospheric warming

ESDD
4, 967–1003, 2013

(Holland and Bitz, 2003; Screen and Simmonds, 2010), but a warming anomaly could also cause additional sea-ice melt in particular during the summer and early autumn season. Thus, influences in both directions are present that could explain the model dependent presence of the lag-1 links.

The relation between AMOC and SIE differs substantially between the models, exhibiting links at zero lag as well as "AMOC → SIE" and "SIE → AMOC" links at time lag 1. A stronger AMOC leads to increased northward heat transport and thus to SIE reduction in the North Atlantic, which could explain the AMOC–SIE links. Levermann et al. (2007) identified increased oceanic heat loss as a result of reduced SIE in the North Atlantic to be a positive feedback on AMOC strength in a CMIP3 model ensemble, implying driving mechanisms that work both ways. Our results indicate that the strength of this individual processes differs substantially between the models investigated. Direct coupling between AMOC and SIE is located in the subpolar and polar Atlantic, while SIE comprises the sea-ice extent over the full Northern Hemisphere. Thus, an AMOC imprint might be present, but not significant in the compound SIE signal. To account for this, we performed the same analysis for SIE limited to the North Atlantic region and found similar results.

3.2 Commonality analysis

In a next step, we use commonality analysis (Seibold and McPhee, 1979) to disentangle AMOC and SIE contributions to GMT variability. Commonality analysis allows to separate the explained variance by a multivariate system into *unique* components that are explained by the individual variables alone and *common* components that give the explained variance by the coupling between them.

As depicted in Fig. 6, the contemporaneous positive AMOC-GMT and negative SIE-GMT links are robust across all models in the ensemble. Therefore, we limit the decomposition of the GMT variability to the AMOC and SIE contribution at lag zero. Following Seibold and McPhee (1979), the unique contribution of AMOC to GMT variability U_{AMOC}

ESDD
4, 967–1003, 2013

derives as

$$U_{\mathrm{AMOC}} = R^2_{\mathrm{FULL}} - R^2_{\mathrm{SIE}}, \quad (3)$$

where R^2_{FULL} is the coefficient of determination (giving the explained variance) for the multivariate regression of the GMT on AMOC and SIE at lag zero. R^2_{SIE} is the explained variance of the univariate regression of GMT on SIE at lag zero. The unique SIE contribution U_{SIE} can be derived accordingly.

The common contribution C is given by the difference between R^2_{FULL} and the sum of the unique contributions. All time series have been standardized. In the ensemble average, we find a unique AMOC contribution of 3 %, SIE 14 % and a common component of 5 %. In total, the coupled AMOC-SIE system contributes about 21 % to GMT variance (see Table 1 for the coefficients of the individual models). We performed the same analysis for low-pass filtered time series and found a decrease in the AMOC unique contribution to 1 %, while the SIE and the common component increase to 21 % and 9 % respectively, in total explaining 31 % of GMT variability.

We would like to emphasize that the analysis presented here is not a comprehensive study of Northern Hemisphere climate variability, since important sources of variability as e.g. multi-decadal variability in the Pacific (Mantua et al., 1997) as well as continental variability are not included. Also interrelations between modes of atmospheric variability such as the North Atlantic and the Arctic oscillation (Hurrell and Deser, 2009) and AMOC as well as SIE, that have been studied intensively and shown to have substantial influence on North Atlantic climate variability (e.g. Tulloch and Marshall, 2012; Frankcombe et al., 2009; Medhaug et al., 2011), are not resolved. However, we find that SIE and AMOC variability already contributes about two thirds to the 33 % explained GMT variance that is found to originate from north of 45° N.

ESDD
4, 967–1003, 2013

4 Deep Ocean heat uptake and density

As shown in the previous section, a significant part of multi-decadal GMT variability is due to changes in the North Atlantic. But when investigating oceanic contributions to GMT variability, not only direct surface feedbacks, but also oceanic heat uptake variability has to be considered (Levitus et al., 2000; Meehl et al., 2011; Balmaseda et al., 2013). As shown in Fig. 1, we find substantial variations in North Atlantic Deep-Ocean (NADO) temperatures (45° to 65° N, z = 1000–2000 m). NADO heat content variability ranges from a standard deviation of 0.16×10^{22} J for the CCSM4 to 0.31×10^{22} J for the CNRM-CM5 model with an ensemble mean of 0.22×10^{22} J. Numbers for the individual models are given in Table 2. Our results compare well with Mauritzen et al. (2012), who find a peak-to-peak variability of about 1×10^{22} J for the entire extratropical North Atlantic deep-ocean (700–2000 m) between 20° to 65° N.

Such anomalies in heat content will also lead to substantial variations in NADO density as depicted in Fig. 7 (red curve). However, density variations caused by temperature change are largely compensated by salinity changes (in blue, inverted) leading to a weaker overall density signal (in black) in line with observational studies (Curry et al., 1998; Yashayaev et al., 2007). Figure 8 depicts the strength of the density compensation and we find substantial variance between the model ensemble (slope of −1 indicates full compensation), ranging from full or even slight overcompensation for the CNRM-CM5 and the CESM1-CAM5 model to only partial compensation in the CCSM4 and the MPI-ESM-LR. Apart from the CNRM-CM5 and the CESM1-CAM5 model, all models show substantial deviation from full compensation (that are significant at one standard deviation except for the CanESM2), indicating a systematic process behind the phenomenon. As shown in Fig. 9, we find deep-ocean density changes to be related to the AMOC in our model ensemble. Except for the CNRM-CM5 model that has a very weak AMOC and exhibits no significant multi-decadal modes of AMOC variability as discussed above, all models show a positive correlation between the AMOC and the NADO thermal density component at zero lag and a significant anti-correlation with

ESDD
4, 967–1003, 2013

a time lag between 10 and 20 yr. Cross-correlations between AMOC and NADO salinity at lag zero are generally weaker over the model ensemble with only the MPI-ESM-LR and -MR as well as the CanESM2 model exhibiting a significant negative peak. Still, most models show a positive correlation at multi-decadal time scales. Taken together, these results indicate that a strong AMOC leads to a NADO warming and salinification on multi-decadal time scales. In the combined density signal, however, only the MPI-ESM-LR model shows a significant AMOC NADO density peak between lag 10 and 20, while a robust correlation at zero lag is found for most models in the ensemble.

Again we performed a time series graph analysis as in Sect. 3.1 to account for the autocorrelations in both time series. Our analysis yields a positive contemporaneous AMOC NADO density link and directed negative AMOC → NADO density links with 5 to 11 yr time lag that are significant at the 99 % level for all models except the CNRM-CM5 (not shown). The robust zero lag link between AMOC and NADO density suggests a causal relation. A linear relationship between meridional density differences and AMOC strength is assumed in conceptual approaches (Stommel, 1961; Rahmstorf, 1996; Johnson et al., 2007; Marzeion and Drange, 2006; Fürst and Levermann, 2012; Cimatoribus et al., 2012) and confirmed by a variety of studies with models of different levels of complexity (e.g., Manabe and Stouffer, 1988; Thorpe et al., 2001; Griesel and Maqueda, 2006; Dijkstra, 2008; Huisman et al., 2010). However, the physical mechanism behind this relationship is controversial in a predominantly geostrophic ocean, although a number of explanations for this in models robustly observed phenomenon have been proposed (Marotzke, 1997; Gnanadesikan, 1999; Schewe and Levermann, 2009; Sijp et al., 2012). Gregory and Tailleux (2011) present a kinetic energy analysis of the AMOC, finding the pressure gradient force to be a dominant driver of the AMOC in the high northern latitudes by conversion of potential to kinetic energy. They report good correlation between changes in the North Atlantic pressure gradient force and the AMOC under CO_2-forced climate change on decadal time scales (their Fig. 10) and find changes in the pressure gradient force to be dominated by buoyancy changes in the northern North Atlantic, which is confirmed by Saenko (2013) for the

ESDD
4, 967–1003, 2013

CanESM2 model. Consequently, they propose a linear relation $\Delta M \propto \Delta\rho$ in the North Atlantic. Such a scaling is also supported by an analytical study by Sijp et al. (2012). Thus, Gregory and Tailleux (2011) provide a physical mechanism for the zero-lag link between NADO and AMOC that is found in all models in the ensemble. Additionally, also a direct feedback between AMOC and NADO temperature and salinity via subpolar convection might play a role. Increased sea surface salinity as a consequence of a strengthened AMOC could lead to enhanced subpolar convection (Mengel et al., 2012) and as a consequence to a deep-ocean freshening and cooling (Yashayaev, 2007).

Based on our findings, we study a conceptual bivariate statistical model for the change in NADO density $\Delta\rho$ and the AMOC change ΔM

$$\begin{aligned} \Delta\rho_t &= a_\rho \Delta\rho_{t-1} + c_{M\rho}\Delta M_{t-\tau} + \epsilon_t^\rho \\ \Delta M_t &= a_M \Delta M_{t-1} + c_{\rho M}\Delta\rho_t + \epsilon_t^M, \end{aligned} \tag{4}$$

with a_ρ and a_M denoting the auto-regressive coefficients and $c_{\rho M}$ and $c_{M\rho}$ the coupling coefficients for $\Delta\rho \rightarrow \Delta M$ at lag zero and $\Delta M \rightarrow \Delta\rho$ with a time lag τ. Results of the fit to the model ensemble time series are given in Table 2. In the ensemble mean, we find about 95 % of the density and about 45 % of the AMOC variance explained by this simple conceptual model, although this good fitting results are partly due to the very strong auto-correlation in the system.

Equation (4) can be written as an auto-regressive system, for which power spectra can be derived analytically (Brockwell and Davis, 2009). Figure 10 depicts analytical spectra for the conceptual model (FULL, green) in comparison with a system without the AMOC-NADO density link (e.g. because of complete density compensation by salinity; $c_{M\rho} = 0$, in blue) and an AR(1) process fitted to the AMOC time series (grey). Note that the $c_{M\rho} = 0$ and AR(1) coefficients may differ from the fully coupled system given in Table 2. We find an enhancement of multi-decadal variability for FULL vs. $c_{M\rho} = 0$ in all models, but only for the MPI-ESM-LR, the CCSM4 and the CESM1-BGC, it also exceeds the spectral density of the fitted AR(1) process for periods be-

ESDD
4, 967–1003, 2013

tween 30 and 70 yr. The MPI-ESM-LR and the CCSM4 show the weakest density compensation in the ensemble with slightly higher values for the CESM1-BGC (compare Fig. 8), indicating that a coupled NADO density-AMOC mode might contribute to multi-decadal variability in models with limited density compensation of temperature and salinity anomalies. All three models also show pronounced spectral peaks with periods below 30 yr likely as a result of other sources of AMOC variability. One possible mechanism is variable Labrador Sea convection that has been found to dominate the 20–yr AMOC mode for the CCSM4 model (Danabasoglu et al., 2012). For the MPI-ESM-MR, the CanESM2 and the CESM1-CAM5, our conceptual model does only show slightly enhanced variability in comparison with a simple AR(1) process, suggesting minor importance of the process. For illustration purposes, we also depict spectra with enhanced AMOC-NADO density coupling ($2 \times c_{M\rho}$ in red, dashed) that show enhanced multi-decadal variability for all models.

As discussed above, a variety of other processes related to horizontal temperature (Te Raa and Dijkstra, 2002), salinity advection (Jungclaus et al., 2005) and atmospheric variability (Eden and Willebrand, 2001) are found to be relevant for multi-decadal AMOC variability and are not included in this simple conceptual system. However, we find substantial changes in the NADO heat content as a result of multi-decadal AMOC variability, that are only partly density compensated in most models. Based on this results, we propose a conceptual model relating NADO density changes and the AMOC and find the coupled system to enhance multi-decadal variability in three models in the ensemble.

5 Discussion and conclusions

By resolving the latitudinal contributions to GMT variance in unperturbed simulations of seven CMIP5 models, we find 33 % of the variance to originate north of 45° N in the ensemble mean, which exceeds the share expected by the surface area. Using a time series graph analysis approach as in Sect. 3.1 (Runge et al., 2012b, 2013), we iden-

ESDD
4, 967–1003, 2013

tify statistically robust couplings between Global Mean Temperature (GMT), Northern Hemisphere Sea Ice Extent (SIE) and the Atlantic meridional overturning circulation (AMOC) at zero lag and find AMOC and SIE to explain about 21 % of GMT variance in the model ensemble mean. Applying commonality analysis in Sect. 3.2, we disentangle AMOC and SIE contributions and report the contribution that can solely be attributed to the AMOC (SIE) alone to be about 3 % (14 %) in the ensemble mean. Additionally, we find AMOC and SIE coupling to explain 5 % of the GMT variance suggesting that coupled AMOC-SIE feedbacks might play an important role for North Atlantic climate variability.

Brönnimann (2009) discusses the influence of natural variability during the early twentieth century warming and highlights the importance of Arctic warming for this global phenomenon. While anthropogenic aerosol emissions affecting patterns of atmospheric variability are discussed as a possible driver of this anomaly (Booth et al., 2012), our results suggest that also natural multi-decadal AMOC variability could have played an important role (Zhang et al., 2013). The Arctic temperature anomaly coincides with a positive AMO-index (Parker et al., 2007) and a sea-ice retreat in the North Atlantic (Macias Fauria et al., 2009; Bengtsson et al., 2004; Semenov and Latif, 2012) that match well with the AMOC-sea-ice coupling identified. The drastic reduction of Northern Hemisphere SIE as a result of anthropogenic global warming (Stroeve et al., 2011, 2012; Notz and Marotzke, 2012), will likely lead to decreased contribution of the high northern latitudes to GMT variability, since SIE is found to be a dominant contributor to GMT variance in an unperturbed climate. Additionally, AMOC-SIE feedbacks might weaken in warmer future climates and consequently also the impact of multi-decadal AMOC variability on GMT might be reduced.

In addition to the AMOC influence on surface temperature variability, we find North Atlantic Deep-Ocean (NADO) heat content to be highly correlated with the AMOC on decadal time scales. Using observational data, Mauritzen et al. (2012) also report a decadal time lag between upper ocean (that is highly correlated with the AMOC at

ESDD
4, 967–1003, 2013

lags between zero and three years in our model ensemble, not shown) and deep-ocean heat content in the northern North Atlantic.

Meehl et al. (2011) investigated deep-ocean heat uptake anomalies during decades exhibiting a hiatus in the GMT over 21st century in global warming model simulations and found a difference of about 1.3×10^{22} J for the global deep-ocean heat uptake rate per decade below 750 m and 0.2×10^{22} J for the Atlantic basin compared to reference decades. We find anomalous NADO heat uptake with a maximum uptake trend of $0.7 \times 10^{22}\,\mathrm{J\,decade^{-1}}$ averaged over the model ensemble with a range from $1.1 \times 10^{22}\,\mathrm{J\,decade^{-1}}$ for the MPI-ESM-LR and 0.5×10^{22} J for the CCSM4, CNRM-CM5 and the CESM1-BGC. Our results indicate that North Atlantic deep-ocean heat uptake anomalies connected to a hiatus decade in GMT increase as identified by Meehl et al. (2011) are very well within the range of natural variability of our model ensemble.

As a consequence of an AMOC strengthening related to a positives AMO signal in the late 1990s (Parker et al., 2007), our analysis would suggest NADO heat content to rise for more than a decade after a peak in circulation strength, which is in good agreement with observations from the North Atlantic (Mauritzen et al., 2012). Studies by Guemas et al. (2013) and Balmaseda et al. (2013) demonstrate that ocean heat uptake plays a crucial role in understanding the GMT hiatus over the last decade. Although they find the dominant signal in the upper Pacific ocean likely related to ENSO variability, also the North Atlantic deep-ocean contributed substantially to anomalous global ocean heat uptake over the last decade (compare Balmaseda et al., 2013, their Fig. S06).

While most of the NADO temperature signal is density-compensated through changes in salinity, we find a substantial model spread regarding the strength of this compensation. We use time-series graph-analysis to extract causal relations out of the highly auto-correlated time series for AMOC and NADO density and found a robust positive link at zero time lag and a negative link between AMOC and NADO density with time lags between 5 and 11 yr (AMOC leads). Based on these results, we propose a stochastic bivariate model that we fit to the time series and find it to explain

ESDD
4, 967–1003, 2013

about 95 % of the density and about 45 % of the AMOC variance in the ensemble average. We report the AMOC-NADO density feedbacks identified to result in enhanced multi-decadal AMOC variability in models with weak density compensation. Thus, they represent a possible advective mechanism for multi-decadal AMOC variability (Latif, 1998; Te Raa and Dijkstra, 2002; Menary et al., 2011).

Acknowledgements. The work was supported by the Federal Ministry for the Environment, Nature Conservation and Nuclear Safety (11 II 093 Global A SIDS and LDCs). Carl-Friedrich Schleussner was funded by the Deutsche Bundesstiftung Umwelt. Jakob Runge appreciates support by the German National Academic Foundation and the DFG grant No. KU34-1. On http://tocsy.pik-potsdam.de/tigramite.php we provide a program with a graphical user interface to estimate the time series graph.

References

Ba, J., Keenlyside, N. S., Park, W., Latif, M., Hawkins, E., and Ding, H.: A mechanism for Atlantic multidecadal variability in the Kiel Climate Model, Clim. Dynam., doi:10.1007/s00382-012-1633-4, online first, 2013. 969

Balmaseda, M. A., Trenberth, K. E., and Källén, E.: Distinctive climate signals in reanalysis of global ocean heat content, Geophys. Res. Lett., 40, 1754–1759, doi:10.1002/grl.50382, 2013. 977, 982

Bengtsson, L., Semenov, V. A., and Johannessen, O. M.: The early twentieth-century warming in the Arctic – a possible mechanism, J. Climate, 17, 4045–4057, 2004. 981

Bentsen, M., Drange, H., Furevik, T., and Zhou, T.: Simulated variability of the Atlantic meridional overturning circulation, Clim. Dynam., 22, 701–720, doi:10.1007/s00382-004-0397-x, 2004. 969

Booth, B. B. B., Dunstone, N. J., Halloran, P. R., Andrews, T., and Bellouin, N.: Aerosols implicated as a prime driver of twentieth-century North Atlantic climate variability., Nature, 484, 228–32, doi:10.1038/nature10946, 2012. 981

Born, A., Stocker, T. F., Raible, C. C., and Levermann, A.: Is the Atlantic subpolar gyre bistable in comprehensive coupled climate models?, Clim. Dynam., 40, 2993–3007, doi:10.1007/s00382-012-1525-7, 2012. 969

ESDD
4, 967–1003, 2013

Brockwell, P. J. and Davis, R. A.: Time series: theory and methods, Springer, New York, 2009. 979
Brönnimann, S.: Early twentieth-century warming, Nat. Geosci., 2, 735–736, doi:10.1038/ngeo670, 2009. 981
Cimatoribus, A. A., Drijfhout, S. S., and Dijkstra, H. A.: Meridional overturning circulation: stability and ocean feedbacks in a box model, Clim. Dynam., online first, doi:10.1007/s00382-012-1576-9, 2012. 978
Curry, R., McCartney, M., and Joyce, T.: Oceanic transport of subpolar climate signals to mid-depth subtropical waters, Nature, 391, 575–577, 1998. 977
Danabasoglu, G., Yeager, S. G., Kwon, Y.-O., Tribbia, J. J., Phillips, A. S., and Hurrell, J. W.: Variability of the Atlantic meridional overturning circulation in CCSM4, J. Climate, 25, 5153–5172, doi:10.1175/JCLI-D-11-00463.1, 2012. 980
Delworth, T. L. and Zeng, F.: Multicentennial variability of the Atlantic meridional overturning circulation and its climatic influence in a 4000 year simulation of the GFDL CM2.1 climate model, Geophys. Res. Lett., 39, 1–6, doi:10.1029/2012GL052107, 2012. 969
Delworth, T., Zhang, R., and Mann, M.: Decadal to centennial variability of the Atlantic from observations and models, ocean circulation: mechanisms and impacts, Geophys. Monogr. Ser., 173, 131–148, 2007. 969
Dijkstra, H. A.: Scaling of the Atlantic meridional overturning circulation in a global ocean model, Tellus A, 60, 749–760, 2008. 978
Dijkstra, H. A., Raa, L., Schmeits, M., and Gerrits, J.: On the physics of the Atlantic multidecadal oscillation, Ocean Dynam., 56, 36–50, doi:10.1007/s10236-005-0043-0, 2006. 969
Dima, M. and Lohmann, G.: Evidence for two distinct modes of large-scale ocean circulation changes over the last century, J. Climate, 23, 5–16, doi:10.1175/2009JCLI2867.1, 2010. 969
Ebert-Uphoff, I. and Deng, Y.: Causal discovery for climate research using graphical models, J. Climate, 25, 5648–5665, doi:10.1175/JCLI-D-11-00387.1, 2012. 970, 973
Eby, M., Weaver, A. J., Alexander, K., Zickfeld, K., Abe-Ouchi, A., Cimatoribus, A. A., Crespin, E., Drijfhout, S. S., Edwards, N. R., Eliseev, A. V., Feulner, G., Fichefet, T., Forest, C. E., Goosse, H., Holden, P. B., Joos, F., Kawamiya, M., Kicklighter, D., Kienert, H., Matsumoto, K., Mokhov, I. I., Monier, E., Olsen, S. M., Pedersen, J. O. P., Perrette, M., Philippon-Berthier, G., Ridgwell, A., Schlosser, A., Schneider von Deimling, T., Shaffer, G., Smith, R. S., Spahni, R., Sokolov, A. P., Steinacher, M., Tachiiri, K., Tokos, K., Yoshimori, M.,

ESDD
4, 967–1003, 2013

Zeng, N., and Zhao, F.: Historical and idealized climate model experiments: an EMIC intercomparison, Clim. Past Discuss., 8, 4121–4181, doi:10.5194/cpd-8-4121-2012, 2012. 968
Eden, C. and Willebrand, J.: Mechanism of interannual to decadal variability of the North Atlantic circulation, J. Climate, 14, 2266–2280, 2001. 969, 980
Fernández-Donado, L., González-Rouco, J. F., Raible, C. C., Ammann, C. M., Barriopedro, D., García-Bustamante, E., Jungclaus, J. H., Lorenz, S. J., Luterbacher, J., Phipps, S. J., Servonnat, J., Swingedouw, D., Tett, S. F. B., Wagner, S., Yiou, P., and Zorita, E.: Large-scale temperature response to external forcing in simulations and reconstructions of the last millennium, Clim. Past, 9, 393–421, doi:10.5194/cp-9-393-2013, 2013. 968
Feulner, G., Rahmstorf, S., Levermann, A., and Volkwardt, S.: On the origin of the surface air temperature difference between the hemispheres in earth's present-day climate, J. Climate, 26, 7136-7150 doi:10.1175/JCLI-D-12-00636.1, 2013. 970
Fidel, J., González-Rouco, L., Gonzalez-Rouco, J. F., Fernández-Donado, L., Raible, C. C., Barriopedro, D., Lutherbacher, J., Jungclaus, J. H., Swingedow, D. Servonnat, J. Zorita, E. Wagner, S., and Ammann, C. M.: Medieval climate anomaly to Little Ice Age transition as simulated by current climate models, Pages News, 19, 3–4, 2011. 968
Frankcombe, L. M., Dijkstra, H. A., and von der Heydt, A.: Noise-induced multidecadal variability in the North Atlantic: excitation of normal modes, J. Phys. Oceanogr., 39, 220–233, doi:10.1175/2008JPO3951.1, 2009. 976
Fürst, J. J., and Levermann, A.: A minimal model for wind- and mixing-driven overturning: threshold behavior for both driving mechanisms, Clim. Dynam., 38, 239–260, doi:10.1007/s00382-011-1003-7, 2012. 978
Gnanadesikan, A.: A simple predictive model for the structure of the oceanic pycnocline, Science, 283, 2077–2079, 1999. 978
Gregory, J. M. and Tailleux, R.: Kinetic energy analysis of the response of the Atlantic meridional overturning circulation to CO_2-forced climate change, Clim. Dynam., 37, 893–914, doi:10.1007/s00382-010-0847-6, 2011. 978, 979
Griesel, A. and Maqueda, M. A. M.: The relation of meridional pressure gradients to North Atlantic deep water volume transport in an ocean general circulation model, Clim. Dynam., 26, 781–799, doi:10.1007/s00382-006-0122-z, 2006. 978
Griffies, S. and Tziperman, E.: A linear thermohaline oscillator driven by stochastic atmospheric forcing, J. Climate, 8, 2440–2453, 1995. 969

ESDD
4, 967–1003, 2013

Guemas, V., Doblas-Reyes, F. J., Andreu-Burillo, I., and Asif, M.: Retrospective prediction of the global warming slowdown in the past decade, Nat. Clim. Change, 3, 649–653, doi:10.1038/nclimate1863, 2013. 982

Hofer, D., Raible, C. C., and Stocker, T. F.: Variations of the Atlantic meridional overturning circulation in control and transient simulations of the last millennium, Clim. Past, 7, 133–150, doi:10.5194/cp-7-133-2011, 2011. 968

Holland, M. M. and Bitz, C. M.: Polar amplification of climate change in coupled models, Clim. Dynam., 21, 221–232, doi:10.1007/s00382-003-0332-6, 2003. 970, 975

Huisman, S. E., den Toom, M., Dijkstra, H. A., and Drijfhout, S.: An indicator of the multiple equilibria regime of the Atlantic meridional overturning circulation, J. Phys. Oceanogr., 40, 551–567, doi:10.1175/2009JPO4215.1, 2010. 978

Hurrell, J. and Deser, C.: North Atlantic climate variability: the role of the North Atlantic Oscillation, J. Marine Syst., 78, 28–41, doi:10.1016/j.jmarsys.2008.11.026, 2009. 976

Johnson, H. L., Marshall, D. P., and Sproson, D. A. J.: Reconciling theories of a mechanically driven meridional overturning circulation with thermohaline forcing and multiple equilibria, Clim. Dynam., 29, 821–836, doi:10.1007/s00382-007-0262-9, 2007. 978

Jones, G. S., Stott, P. A., and Christidis, N.: Attribution of observed historical near-surface temperature variations to anthropogenic and natural causes using CMIP5 simulations, J. Geophys. Res.-Atmos., 118, 4001–4024, doi:10.1002/jgrd.50239, 2013. 970

Jungclaus, J., Haak, H., Latif, M., and Mikolajewicz, U.: Arctic–North Atlantic interactions and multidecadal variability of the meridional overturning circulation, J. Climate, 18, 4013–4031, 2005. 969, 980

Knight, J. R., Allen, R. J., Folland, C. K., Vellinga, M., and Mann, M. E.: A signature of persistent natural thermohaline circulation cycles in observed climate, Geophys. Res. Lett., 32, L20708, doi:10.1029/2005GL024233, 2005. 969, 970

Knight, J. R., Folland, C. K., and Scaife, A. A.: Climate impacts of the Atlantic multidecadal oscillation, Geophys. Res. Lett., 33, L17706, doi:10.1029/2006GL026242, 2006. 970

Knudsen, M. F., Seidenkrantz, M.-S., Jacobsen, B. H., and Kuijpers, A.: Tracking the Atlantic Multidecadal Oscillation through the last 8,000 years, Nat. Comm., 2, 178, doi:10.1038/ncomms1186, 2011. 968

Latif, M.: Dynamics of interdecadal variability in coupled ocean – atmosphere models, J. Climate, 11, 602–624, 1998. 983

ESDD
4, 967–1003, 2013

Lee, S. and Wang, C.: Delayed advective oscillation of the Atlantic thermohaline circulation, J. Climate, 23, 1254, doi:10.1175/2009JCLI3339.1, 2010. 969
Levermann, A. and Born, A.: Bistability of the subpolar gyre in a coarse resolution climate model, Geophys. Res. Lett., 34, L24605, doi:10.1029/2007GL031732, 2007. 969
Levermann, A., Mignot, J., Nawrath, S., and Rahmstorf, S.: The role of Northern Sea ice cover for the weakening of the thermohaline circulation under global warming, J. Climate, 20, 4160–4171, doi:10.1175/JCLI4232.1, 2007. 975
Levitus, S., Antonov, J., Boyer, T., and Stephens, C.: Warming of the world ocean, Science, 287, 2225–2229, doi:10.1126/science.287.5461.2225, 2000. 977
Macias Fauria, M., Grinsted, A., Helama, S., Moore, J., Timonen, M., Martma, T., Isaksson, E., and Eronen, M.: Unprecedented low twentieth century winter sea ice extent in the Western Nordic Seas since A. D. 1200, Clim. Dynam., 34, 781–795, doi:10.1007/s00382-009-0610-z, 2009. 981
Manabe, S. and Stouffer, R. J.: Two stable equilibria of a coupled ocean-atmosphere model, J. Climate, 1, 841–866, 1988. 978
Mantua, N. J., Hare, S. R., Zhang, Y., Wallace, J. M., and Francis, R. C.: A Pacific interdecadal climate oscillation with impacts on salmon production, B. Am. Meteorol. Soc., 78, 1069–1079, 1997. 976
Marotzke, J.: Boundary mixing and the dynamics of three-dimensional thermohaline circulations, J. Phys. Oceanogr., 27, 1713–1728, 1997. 978
Marzeion, B. and Drange, H.: Diapycnal mixing in a conceptual model of the Atlantic meridional overturning circulation, Deep-Sea Res. Pt. II, 53, 226–238, 2006. 978
Mauritzen, C., Melsom, A., and Sutton, R. T.: Importance of density-compensated temperature change for deep North Atlantic Ocean heat uptake, Nat. Geosci.,5, 905–910, doi:10.1038/ngeo1639, 2012. 977, 981, 982
Medhaug, I., Langehaug, H. R., Eldevik, T., Furevik, T., and Bentsen, M.: Mechanisms for decadal scale variability in a simulated Atlantic meridional overturning circulation, Clim. Dynam., 39, 77–93, doi:10.1007/s00382-011-1124-z, 2011. 969, 976
Meehl, G. A., Arblaster, J. M., Fasullo, J. T., Hu, A., and Trenberth, K. E.: Model-based evidence of deep-ocean heat uptake during surface-temperature hiatus periods, Nat. Clim. Change, 1, 360–364, doi:10.1038/nclimate1229, 2011. 977, 982
Menary, M. B., Park, W., Lohmann, K., Vellinga, M., Palmer, M. D., Latif, M., and Jungclaus, J. H.: A multimodel comparison of centennial Atlantic meridional overturning circu-

ESDD
4, 967–1003, 2013

lation variability, Clim. Dynam., 38, 2377–2388, doi:10.1007/s00382-011-1172-4, 2011. 969, 983
Mengel, M., Levermann, A., Schleussner, C.-F., and Born, A.: Enhanced Atlantic subpolar gyre variability through baroclinic threshold in a coarse resolution model, Earth Syst. Dynam., 3, 189–197, doi:10.5194/esd-3-189-2012, 2012. 969, 979
Mohino, E., Janicot, S., and Bader, J.: Sahel rainfall and decadal to multi-decadal sea surface temperature variability, Clim. Dynam., 37, 419–440, doi:10.1007/s00382-010-0867-2, 2010. 969
Notz, D. and Marotzke, J.: Observations reveal external driver for Arctic sea-ice retreat, Geophys. Res. Lett., 39, L08502, doi:10.1029/2012GL051094, 2012. 981
Ortega, P., Montoya, M., González-Rouco, F., Mignot, J., and Legutke, S.: Variability of the Atlantic meridional overturning circulation in the last millennium and two IPCC scenarios, Clim. Dynam., 38, 1925–1947, doi:10.1007/s00382-011-1081-6, 2011. 968
Otterå, O., Bentsen, M., Drange, H., and Suo, L.: External forcing as a metronome for Atlantic multidecadal variability, Nat. Geosci., 3, 688–694, doi:10.1038/ngeo955, 2010. 968
Park, W. and Latif, M.: Multidecadal and multicentennial variability of the meridional overturning circulation, Geophys. Res. Lett., 35, L22703, doi:10.1029/2008GL035779, 2008. 969
Park, W. and Latif, M.: Atlantic Meridional Overturning Circulation response to idealized external forcing, Clim. Dynam., 39, 1709–1726, doi:10.1007/s00382-011-1212-0, 2011. 969
Parker, D., Folland, C., Scaife, A., Knight, J., Colman, A., Baines, P., and Dong, B.: Decadal to multidecadal variability and the climate change background, J. Geophys. Res., 112, 1–18, doi:10.1029/2007JD008411, 2007. 981, 982
Persechino, A., Marsh, R., Sinha, B., Megann, A. P., Blaker, A. T., and New, A. L.: Decadal-timescale changes of the Atlantic overturning circulation and climate in a coupled climate model with a hybrid-coordinate ocean component, Clim. Dynam., 39, 1021–1042, doi:10.1007/s00382-012-1432-y, 2012. 969
Rahmstorf, S.: On the freshwater forcing and transport of the Atlantic thermohaline circulation, Clim. Dynam., 12, 799–811, 1996. 978
Runge, J., Heitzig, J., Marwan, N., and Kurths, J.: Quantifying causal coupling strength: a lag-specific measure for multivariate time series related to transfer entropy, Phys. Rev. E, 86, 061121, doi:10.1103/PhysRevE.86.061121, 2012a. 970, 973

ESDD
4, 967–1003, 2013

Runge, J., Heitzig, J., Petoukhov, V., and Kurths, J.: Escaping the curse of dimensionality in estimating multivariate transfer entropy, Phys. Rev. Lett., 108, 1–5, doi:10.1103/PhysRevLett.108.258701, 2012b. 973, 974, 980, 999

Runge, J., Petoukhov, V., and Kurths, J.: Quantifying the strength and delay of climatic interactions: the ambiguities of cross correlation and a novel graphical models based measure, J. Climate, submitted, 2013. 972, 973, 980

Saenko, O.: Energetics of weakening and recovery of the Atlantic overturning in a climate change simulation, Geophys. Res. Lett., 40, 888–892, doi:10.1002/grl.50101, 2013. 978

Schewe, J. and Levermann, A.: The role of meridional density differences for a wind-driven overturning circulation, Clim. Dynam., 34, 547–556, doi:10.1007/s00382-009-0572-1, 2009. 978

Schlesinger, M. and Ramankutty, N.: An oscillation in the global climate system of period 65–70 years, Nature, 367, 723–726, doi:10.1038/367723a0, 1994, 1994. 968

Screen, J. A. and Simmonds, I.: The central role of diminishing sea ice in recent Arctic temperature amplification, Nature, 464, 1334–1337, doi:10.1038/nature09051, 2010. 970, 975

Seibold, D. and McPhee, R.: Commonality analysis: a method for decomposing explained variance in multiple regression analyses, Human Comm. Res., 5, 355–365, 1979. 970, 975

Semenov, V. A. and Latif, M.: The early twentieth century warming and winter Arctic sea ice, The Cryosphere, 6, 1231–1237, doi:10.5194/tc-6-1231-2012, 2012. 981

Sévellec, F., and Fedorov, A. V.: The leading, interdecadal eigenmode of the Atlantic meridional overturning circulation in a realistic ocean model, J. Climate, 26, 2160–2183, doi:10.1175/JCLI-D-11-00023.1, 2013. 969

Sijp, W. P., Gregory, J. M., Tailleux, R., and Spence, P.: The key role of the western boundary in linking the AMOC strength to the north–south pressure gradient, J. Phys. Oceanogr., 42, 628–643, doi:10.1175/JPO-D-11-0113.1, 2012. 978, 979

Stommel, H.: Thermohaline convection with two stable regimes of flow, Tellus, 13, 224–230, 1961. 978

Stroeve, J. C., Serreze, M. C., Holland, M. M., Kay, J. E., Malanik, J., and Barrett, A. P.: The Arctic's rapidly shrinking sea ice cover: a research synthesis, Clim. Change, 110, 1005–1027, doi:10.1007/s10584-011-0101-1, 2011. 981

Stroeve, J. C., Kattsov, V., Barrett, A., Serreze, M., Pavlova, T., Holland, M., and Meier, W. N.: Trends in Arctic sea ice extent from CMIP5, CMIP3 and observations, Geophys. Res. Lett., 39, L16502, doi:10.1029/2012GL052676, 2012. 981

ESDD
4, 967–1003, 2013

Taylor, K. E., Stouffer, R. J., and Meehl, G. A.: An overview of CMIP5 and the experiment design, B. Am. Meteorol. Soc., 93, 485–498, 2012. 970

Te Raa, L. A. and Dijkstra, H. A.: Instability of the thermohaline ocean circulation on interdecadal timescales, J. Phys. Oceanogr., 32, 138–160, 2002. 969, 980, 983

Thorpe, R., Gregory, J., and Johns, T.: Mechanisms determining the Atlantic thermohaline circulation response to greenhouse gas forcing in a non-flux-adjusted coupled climate model, J. Climate, 14, 3102–3116, 2001. 978

Timmermann, A. and Latif, M.: Northern hemispheric interdecadal variability: a coupled air–sea mode, J. Climate, 11, 1906–1931, 1998. 969

Tulloch, R. and Marshall, J.: Exploring mechanisms of variability and predictability of Atlantic meridional overturning circulation in two coupled climate models, J. Climate, 25, 4067–4080, doi:10.1175/JCLI-D-11-00460.1, 2012. 969, 976

Vimont, D. J. and Kossin, J. P.: The Atlantic Meridional Mode and hurricane activity, Geophys. Res. Lett., 34, L07709, doi:10.1029/2007GL029683, 2007. 969

Wouters, B., Drijfhout, S., and Hazeleger, W.: Interdecadal North-Atlantic meridional overturning circulation variability in EC-EARTH, Clim. Dynam., 39, 2695–2712, doi:10.1007/s00382-012-1366-4, 2012. 969

Yashayaev, I.: Hydrographic changes in the Labrador Sea, 1960–2005, Prog. Oceanogr., 73, 242–276, doi:10.1016/j.pocean.2007.04.015, 2007. 979

Yashayaev, I., van Aken, H. M., Holliday, N. P., and Bersch, M.: Transformation of the Labrador sea water in the subpolar North Atlantic, Geophys. Res. Lett., 34, L22605, doi:10.1029/2007GL031812, 2007. 977

Zanchettin, D., Rubino, A., and Jungclaus, J. H.: Intermittent multidecadal-to-centennial fluctuations dominate global temperature evolution over the last millennium, Geophys. Res. Lett., 37,L14702, doi:10.1029/2010GL043717, 2010. 970

Zhang, R. and Delworth, T. L.: A new method for attributing climate variations over the Atlantic Hurricane Basin's main development region, Geophys. Res. Lett., 36, L06701, doi:10.1029/2009GL037260, 2009. 969

Zhang, R., Delworth, T., and Held, I.: Can the Atlantic Ocean drive the observed multidecadal variability in Northern Hemisphere mean temperature?, Geophys. Res. Lett., 34, L02709, doi:10.1029/2006GL028683, 2007. 970

ESDD
4, 967–1003, 2013

Zhang, R., Delworth, T. L., Sutton, R., Hodson, D. L., Dixon, K. W., Held, I. M., Kushnir, Y., Marshall, J., Ming, Y., and Msadek, R.: Have aerosols caused the observed Atlantic multidecadal variability?, J. Atmos. Sci., 70, 1135–1144, doi:10.1175/JAS-D-12-0331.1, 2013. 981

ESDD
4, 967–1003, 2013

Table 1. Results of the commonality analysis of GMT variability and the AMOC and SIE contribution at lag zero. U_{AMOC} and U_{SIE} denote the unique AMOC and SIE contribution and C the common component. R^2_{FULL} gives the explained GMT variance by the coupled system. The middle column denotes the explained GMT variance integrated over the Northern Hemisphere north of 45° N as in Fig. 3. North Atlantic Deep-Ocean (NADO) (45° to 65° N, z = 1000–2000 m) heat content (OHC) variability over the model ensemble is given on the right. First column: standard deviation of the time series, second column: maximum decadal trend over the full time series.

	U_{AMOC}	U_{SIE}	C	R^2_{FULL}	SAT > 45° N	OHC STD [10^{22} J]	OHC RATE [10^{22} J dec^{-1}]
MPI-ESM-LR	0.01	0.13	0.03	0.16	0.27	0.20	1.1
MPI-ESM-MR	0.02	0.09	0.05	0.16	0.27	0.21	1.0
CanESM2	< 0.01	0.20	0.01	0.21	0.33	0.23	0.6
CNRM-CM5	0.02	0.18	0.06	0.26	0.33	0.31	0.5
CCSM4	0.06	0.08	0.03	0.17	0.36	0.16	0.5
CESM1-BGC	0.06	0.07	0.05	0.19	0.39	0.20	0.5
CESM1-CAM5	0.02	0.22	0.08	0.32	0.39	0.22	0.7
Mean	0.03	0.14	0.05	0.21	0.33	0.22	0.7

ESDD
4, 967–1003, 2013

Table 2. Results of the multivariate regression of the conceptual coupled AMOC-NADO density system as in Eq. (4) to the individual models.

	a_ρ	$c_{M\rho}$	a_M	$c_{\rho M}$	σ_ρ^2	σ_M^2	$\sigma_{M\rho}$	τ	R_M^2	R_ρ^2
MPI-ESM-LR	0.98 ± 0.01	-0.08 ± 0.01	0.61 ± 0.03	0.18 ± 0.03	0.07	0.48	0.04	7.0	0.52	0.93
MPI-ESM-MR	0.99 ± 0.01	-0.06 ± 0.01	0.57 ± 0.03	0.13 ± 0.03	0.05	0.59	0.07	8.0	0.40	0.95
CanESM2	1.01 ± 0.01	-0.07 ± 0.01	0.64 ± 0.03	0.13 ± 0.03	0.03	0.49	0.03	6.0	0.51	0.97
CCSM4	1.01 ± 0.01	−0.11 ± 0.01	0.37 ± 0.04	0.38 ± 0.04	0.07	0.56	0.05	5.0	0.45	0.93
CESM1-BGC	0.97 ± 0.01	−0.05 ± 0.01	0.3 ± 0.04	0.39 ± 0.04	0.08	0.64	0.05	11.0	0.36	0.92
CESM1-CAM5	1.02 ± 0.01	−0.07 ± 0.01	0.49 ± 0.05	0.24 ± 0.05	0.03	0.56	0.04	6.0	0.45	0.97
Mean	1.0	−0.07	0.5	0.24	0.05	0.55	0.05	7.2	0.45	0.95

ESDD
4, 967–1003, 2013

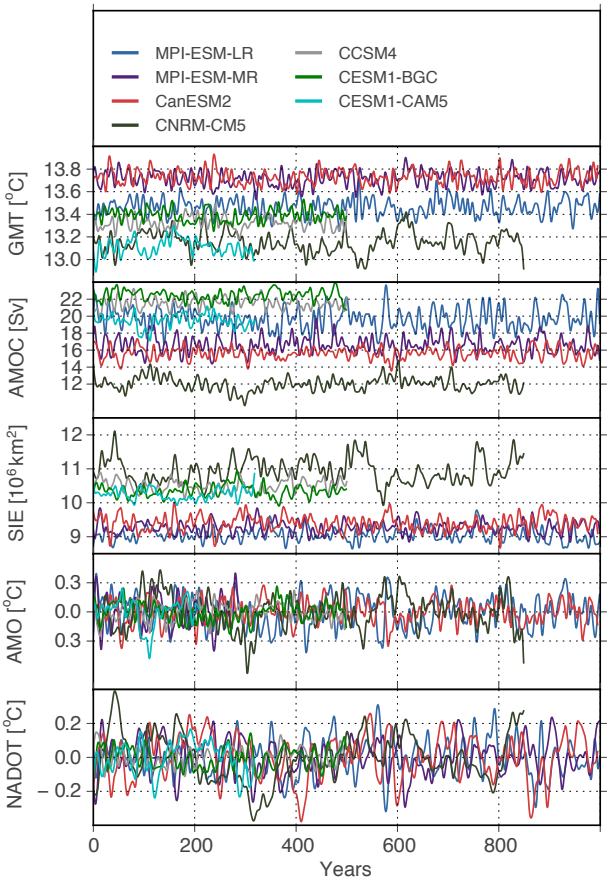

Fig. 1. Time series for GMT, AMOC, Northern Hemisphere Sea-Ice Extent (SIE), the Atlantic multi-decadal oscillation (AMO) index and North Atlantic deep-ocean (NADO) temperature for seven CMIP5 models. A 10 yr butterworth low-pass filter is applied to the time series before plotting.

ESDD
4, 967–1003, 2013

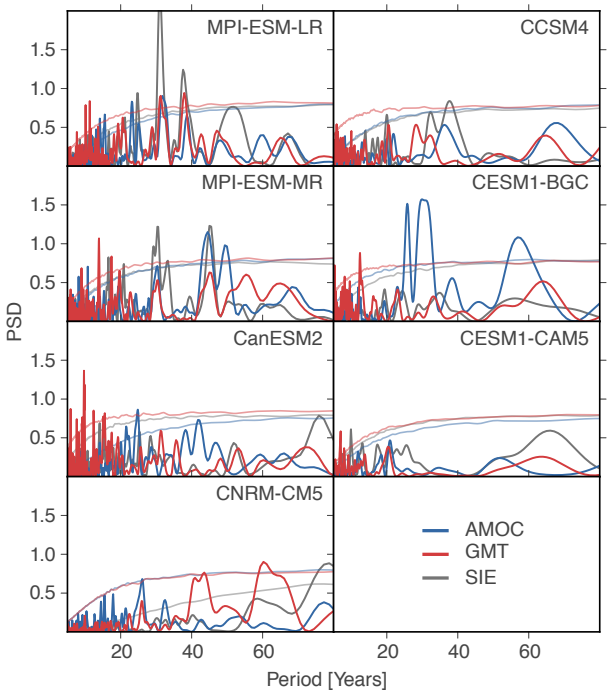

Fig. 2. Power spectral density of AMOC (blue), GMT (red) and SIE (grey). Light lines indicate the 95 % significance levels of a fitted red noise first order auto-regressive process. In this plot, all amplitudes are rescaled relative to the corresponding maximum of the 95 % significance level.

ESDD
4, 967–1003, 2013

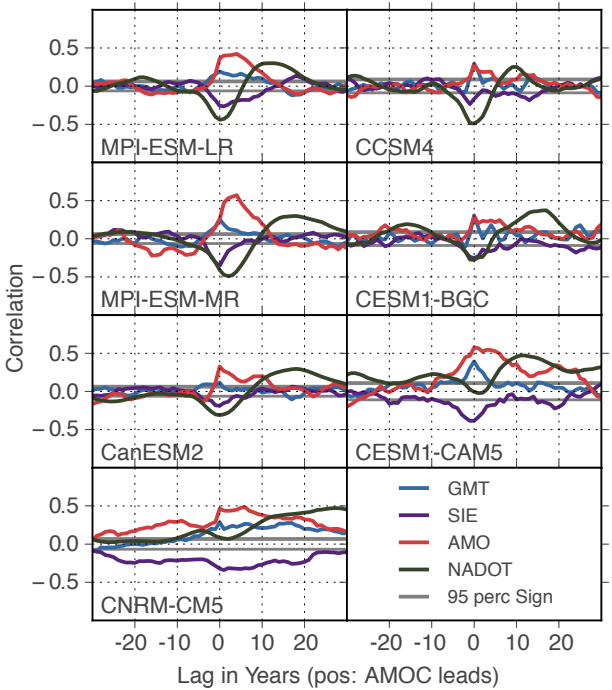

Fig. 3. Cross correlations between AMOC and GMT, SIE, NADO temperature and the AMO index (positive: AMOC leads). The grey lines mark the two-tailed 95 % significance range.

ESDD
4, 967–1003, 2013

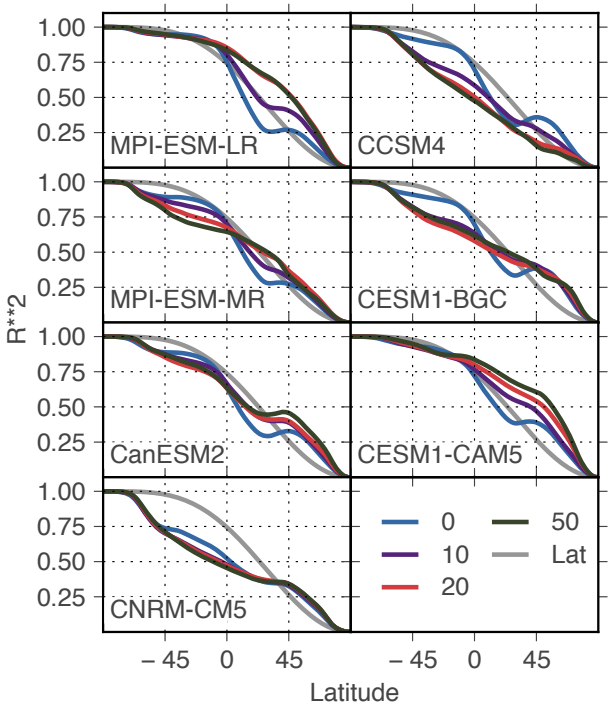

Fig. 4. Meridional dependence of the GMT variance. The horizontal averaged yearly SAT anomalies are integrated from 90° N southward. The value for a given latitude marks the explained variance (R^2) of the GMT time series by the integrated SAT variance north of it. Colors indicate different low-pass filters applied. The grey line marks the variance contribution assuming equally distributed GMT variance. The explained variances of the unfiltered GMT signal that originates from north of 45° N are listed in Table 1.

ESDD
4, 967–1003, 2013

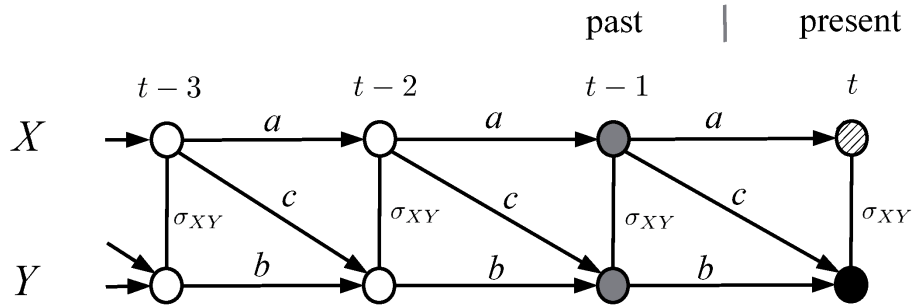

Fig. 5. Representation of the time series graph of the simple coupled bivariate process (X_t, Y_t) in Eq. (1) with the constant coefficients a, b and c. σ_{XY} is the non-diagonal element of the covariance matrix. Process Y_t (black node) is driven by Y_{t-1} and X_{t-1} (in grey) and has a contemporaneous link to X_t (hatched). Due to stationarity, the same causal relation holds for all t.

ESDD
4, 967–1003, 2013

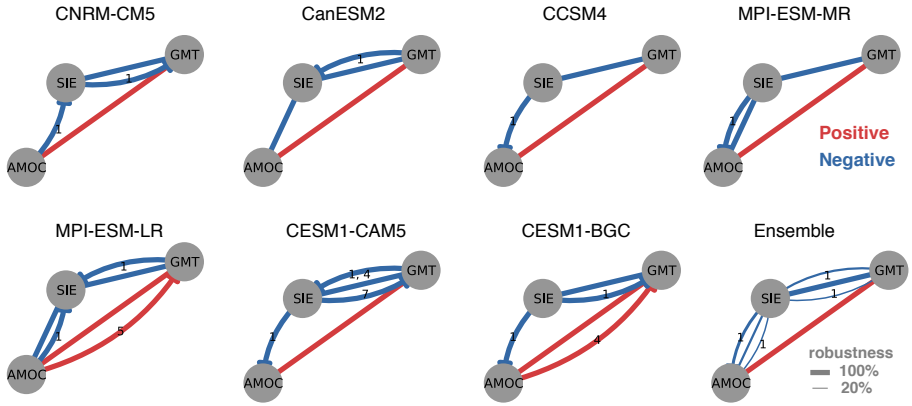

Fig. 6. Resulting time series graphs for AMOC, GMT and SIE by applying a method introduced in Runge et al. (2012b). Based on the sign of the partial correlation as a result of the graph estimation algorithm, we denote positive (negative) partial correlations in red (blue). Direct links are indicated by curved lines (numbers denote different time lags), whereas straight lines represent contemporaneous links at lag zero.

ESDD
4, 967–1003, 2013

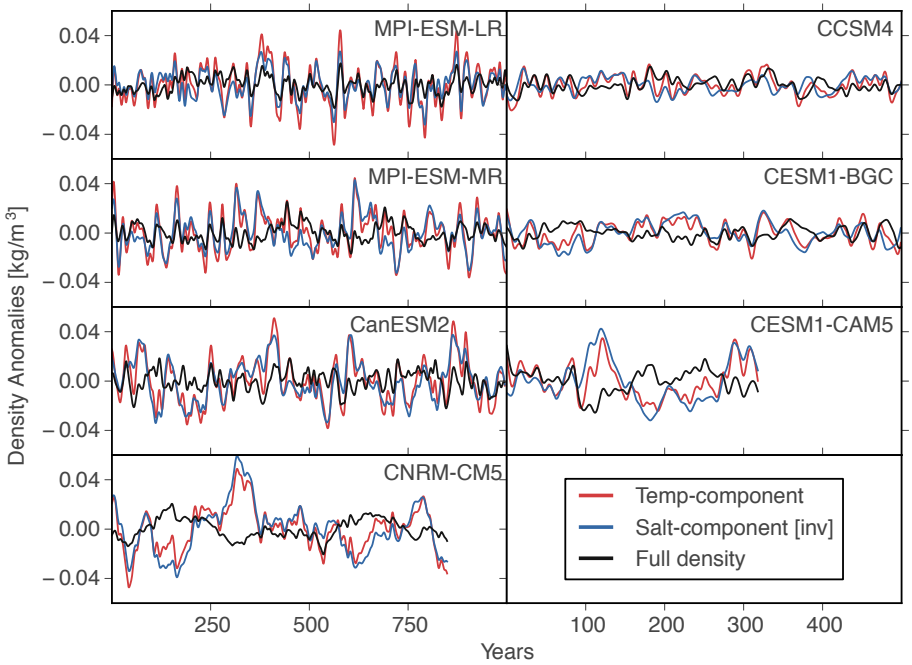

Fig. 7. North Atlantic Deep Ocean density time series (black) and its salinity (blue, inverted) and temperature (red) related components.

ESDD
4, 967–1003, 2013

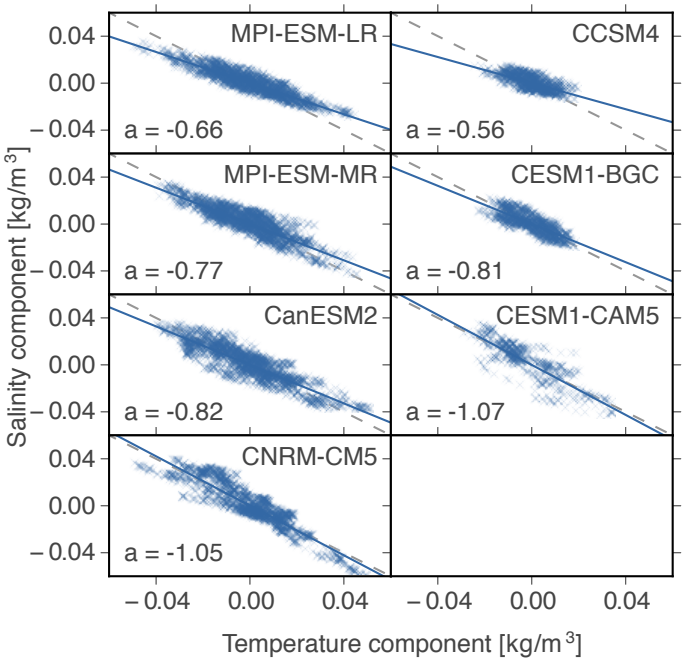

Fig. 8. Relation of temperature and salinity driven NADO density changes. The blue line marks the linear fit with slope *a*. The $a = -1$ line is drawn in grey.

ESDD
4, 967–1003, 2013

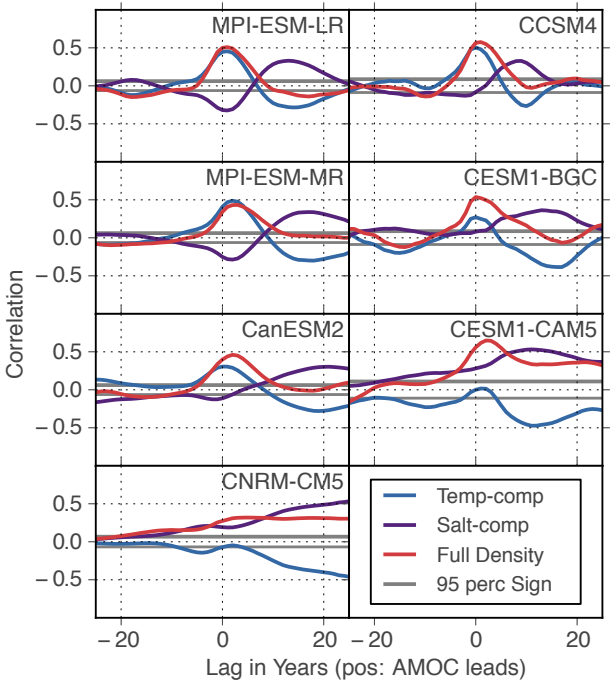

Fig. 9. Cross correlations between AMOC and NADO density and its temperature and salinity related components (positive: AMOC leads). The grey lines mark the two-tailed 95 % significance range.

ESDD
4, 967–1003, 2013

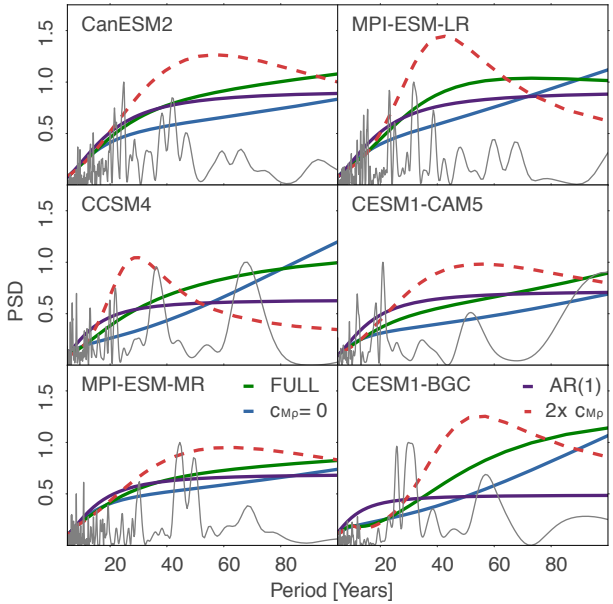

Fig. 10. Analytically derived power spectral densities for different model systems regressed on the individual model time series: (1) fully coupled AMOC-NADO density system (green), (2) decoupled system $c_{m\rho} = 0$ (blue), (3) AR(1) process (purple) and a doubled AMOC–NADO coupling ($2 \times c_{m\rho}$, dashed red). AMOC spectra derived from the model time series rescaled relative to their maximum amplitude are shown in light grey.

ESDD
4, 967–1003, 2013